The Journal of Physical Chemistry

 VOLUME 100, NUMBER 32, AUGUST 8, 1996

LETTERS

Structure, Dynamics, and Thermodynamics of Passivated Gold Nanocrystallites and Their Assemblies

W. D. Luedtke and Uzi Landman*

School of Physics, Georgia Institute of Technology, Atlanta, Georgia 30332

Received: June 12, 1996[⊗]

The structure, dynamics, and thermodynamics of gold nanocrystallites passivated by alkylthiolate monolayers were investigated, using molecular dynamics simulations, in different environments—as isolated gas-phase clusters, when adsorbed on a graphite surface, and when assembled into three-dimensional superlattices. The packing arrangements and densities of the monolayers passivating the facets of the core gold nanocrystallites differ from those found on extended gold surfaces, exhibiting organization into molecular bundles of preferred orientations which upon heating undergo a reversible melting transition from the ordered bundled state to a uniform intermolecular orientational distribution. The equilibrium geometries of adsorbed nanocrystallites depend on the chain length of the passivating molecules which effectively lubricate the interface between the gold core and the graphite surface conferring high surface mobility to the crystallites, involving a collective slip-diffusion mechanism. The room-temperature equilibrium structure of the superlattice made of $Au_{140}(C_{12}H_{25}S)_{62}$ nanocrystallites is predicted to be tetragonally distorted fcc with enhanced orientational bundling of the passivating molecules along the direction of the tetragonal distortion. The cohesion of the superlattice derives dominantly from the interactions between the interlocking molecular bundles. On the other hand, passivation by shorter chain molecules, $Au_{140}(C_4H_9S)_{62}$, results in a room-temperature body-centered cubic superlattice structure, transforming to a fcc lattice at higher temperatures.

Characterization and elucidation of size-evolutionary patterns of the properties of finite materials aggregates exhibiting discrete quantized energy level spectra and specific structures and morphologies, investigations of unique properties of finite-size materials clusters, and studies of the nature of the evolution from the molecular and cluster regimes to the bulk phase are among the major challenges of modern materials science and have been the subject of intensive research endeavors. These investigations, which include explorations of structural, electronic, thermodynamic, spectroscopic, and chemical properties of isolated clusters and their assemblies,[1] have revealed unique size-dependent physical and chemical materials phenomena differing from those found in the bulk, motivating some to classify such materials aggregates of reduced dimensions as a distinct state of matter. Furthermore, nanophase materials built through the assembly of nanometer-scale units into ordered superlattices offer exciting perspectives as novel materials whose optical, electronic, and transport properties may be controlled by the selection of the composition and sizes of the building-block units, suggesting their potential utilization as components in electronic, optoelectronic, and sensor technologies.

Preparation of such materials often requires passivation of the individual "building blocks" to inhibit their propensity to agglomerate and sinter. Indeed, it has been demonstrated recently[2−7] that nanocrystalline gold molecules and their two- and three-dimensional crystalline superlattices can be prepared through solution- or gas-phase methods, with effective passivation of the surfaces of the individual crystallites by self-assembling monolayers (SAMs) of alkyl thiolates (RS, where $R = C_nH_{2n+1}$ and S is a sulfur atom binding to the gold atoms).[8] In one of these studies,[4] it has been shown, using an arsenal of

[⊗] Abstract published in *Advance ACS Abstracts,* July 15, 1996.

S0022-3654(96)01721-2 CCC: $12.00

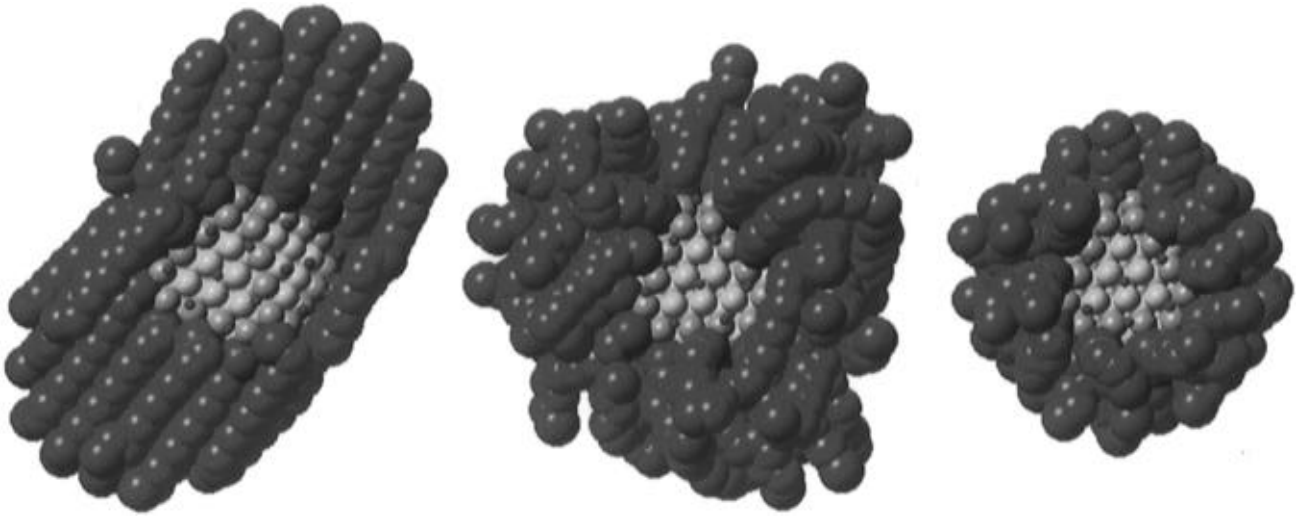

Figure 1. Equilibrium configurations of passivated Au_{140} isolated crystallites. The structures at the left and middle correspond to low- (200 K) and high-temperature (350 K) configurations for $Au_{140}(C_{12}H_{25}S)_{62}$ illustrating "bundling" at low temperature, and the structure on the right is for $Au_{140}(C_4H_9S)_{62}$ at 300 K. Part of the thiol monolayer was removed to expose (111) and (100) facets of the underlying TO^+ Au_{140} crystallite. Yellow and red spheres represent Au and S atoms; green spheres correspond to alkyl segments and the methyls at the chain ends are colored in darker green.

theoretical and experimental techniques (including molecular dynamics (MD) simulations and structural optimizations, mass spectrometry, high-resolution electron microscopy, and X-ray diffraction), that gold nanocrystals form a discrete self-selecting energetically optimal structural sequence whose members have face-centered cubic (fcc) lattices with morphologies of a truncated-octahedral (TO) motif.[4,9]

We report on structural, dynamic, and thermodynamic properties of passivated gold nanocrystallites $Au_N(RS)_M$, with $N = 140$, 201, 459, and 586 (corresponding to some members of the Au_N optimal sequence) and R = C_4H_9 or $C_{12}H_{25}$, in different environments: as isolated gas-phase clusters, when adsorbed on a graphite surface, and when assembled into three-dimensional (3D) superlattices. While the properties of SAMs on extended metal (gold) surfaces have been studied extensively,[10−13] this is the first theoretical investigation of such systems involving finite crystallites.[4,9] We find that such surfactants form compact monolayers whose unique structures and packing are influenced by the finite nature of the crystallites, differing from those found on extended gold surfaces.[10−13] The surfactant monolayers on isolated crystallites undergo a phase transition near the bulk melting temperature of the alkane residue of the corresponding alkyl thiolate, accompanied by intramolecular conformational changes. At low temperatures the passivating dodecanethiol monolayer is "bundled" into groups of molecules with a preferential "parallel" intermolecular orientation of the molecular backbones in each bundle, and the bundles themselves are preferentially oriented with respect to each other. The equilibrium adsorption geometries of isolated $Au_{140}(RS)_{62}$ crystallites on graphite are found to depend on the alkanethiol chain length. The molecules of the passivating monolayers lubricate effectively the interface between the adsorbed crystallite and the underlying surface resulting in surprisingly high surface mobilities of the crystallites, occurring through an activated collective slip-diffusion mechanism. The structures of the three-dimensional superlattices formed by the passivated nanocrystallites are found to depend on the chain length of the surfactant molecules and on the temperature. Thus, passivation by long chain thiols results at room temperature in a tetragonal fcc (t-fcc) superlattice made of $Au_{140}(C_{12}H_{25}S)_{62}$ units, with the cohesion of the superlattice deriving dominantly from van der Waals interactions between interlocking bundles of the passivating molecules oriented preferentially along the direction of the tetragonal distortion. On the other hand, a bcc superlattice of $Au_{140}(C_4H_9S)_{62}$ is predicted at temperatures up to $T \approx 300$ K, undergoing a reversible transformation to a fcc lattice at higher temperatures.

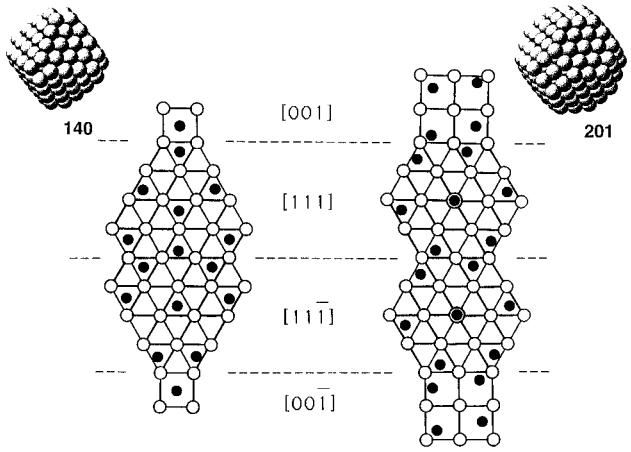

Figure 2. Arrangement of the sulfurs (filled circles) on the facets (gold atoms shown as open circles) of the equilibrium structures of isolated $Au_{140}(TO^+)$ and $Au_{201}(TO)$ crystallites, at left and right, respectively. The corresponding structures of the crystallites are shown as insets. The nearest-neighbor distance between Au atoms is ∼2.8 Å. For $Au_{140}(RS)_{62}$ the inequivalent S−S distances are 3.9 and 4.5 Å (on the (111) facets), and for $Au_{201}(RS)_{80}$ the S−S distances are 4.1 Å (on the (001) facets) and 4.3 Å (on the (111) facets).

The interactions used in our MD simulations include united-atom model potentials (nonbonded, bond-stretch, bond-angle, and dihedral terms) describing intra- and intermolecular interactions of the alkyl (CH_2 and CH_3) segments;[14] a sulfur-to-gold interatomic Morse potential fitted to calculated binding energies, equilibrium distances, and vibrational force constants of alkyl thiolates adsorbed on Au(111) and Au(100) surfaces;[15] sulfur−sulfur and sulfur to alkyl-segment interaction potentials;[16] and an alkyl-segment to Au atom interaction potential fitted to desorption data of alkanes from metal surfaces.[17] These interaction potentials were tested by us in simulations of dodecane thiols adsorbed on extended close-packed gold surfaces, yielding results for structural and thermodynamic properties in satisfactory agreement with experimental data (that is, packing density, tilt angles, molecular conformations, melting

transition, desorption energy, and mechanical response characteristics). Many-body embedded-atom potentials were employed in optimizing the structures of the bare gold clusters.[9,18] In simulations of nanocrystallites adsorbed on graphite, the interactions between the alkane segments and the graphite atoms were described following ref 19, and those between the gold atoms and the graphite surface were modeled using 6−12 Lennard-Jones potentials with the "mixing rules" given in ref 14.

Preparation of the passivated clusters followed the following procedure: (i) the bare Au_n cluster in its optimal geometry[4,9] was surrounded by a large sphere with a reflecting boundary which was filled with butanethiol molecules in large excess compared to the number required to form a compact monolayer. The system was allowed to evolve at a very low temperature, resulting in condensation of the molecules onto the cluster. (ii) The temperature was then increased to $T = 200$ K and subsequently to 300, 400, and briefly to 500 K and was cycled between these temperatures to allow desorption of excess molecules and exploration of stable binding sites. This procedure resulted in equilibrated well-annealed compact monolayers on the gold clusters (see Figure 1 for representative structures); in simulations of dodecanethiol monolayers the alkyl residues of the butanethiols were replaced by $R = C_{12}H_{25}$ once a compact monolayer was formed and the system was allowed to equilibrate further.

Structures and Thermodynamics of Isolated Passivated Gold Nanocrystallites. SAMs form ordered structures on the low-index faces of extended gold surfaces; for example, the translational correlation distance in a monolayer of docosanethiol on Au(111) is 60 Å and on Au(100) it is 130−200 Å.[20] The adsorption sites and packing of the thiols depend on the Au surface[10] (calculated per molecule areas of 21.4 and 20.6 Å^2 on Au(111) and Au(100), respectively), and the axes of the adsorbed alkyl chains are tilted with respect to the surface normal by 20−35°.[10]

The dependence of the overlayer arrangement on the structure of the underlying surface is further complicated in the case of SAMs adsorbed on finite crystalline gold clusters which expose adjoining (111) and (100) facets. We found that the arrangement of the molecules on such clusters is different from that found on extended Au surfaces and depends on the size of the cluster. To illustrate, we show in Figure 2 the arrangement of the sulfur atoms in $Au_{140}(RS)_{62}$ and $Au_{201}(RS)_{80}$. For the smaller cluster (whose morphology is designated TO^+ indicating an irregular truncated octahedron with the number of gold atoms on an edge adjoining two (111) facets $m = 4$, and that on an edge adjoining a (111) and a (100) facet $n = 2$, see left inset in Figure 2), the sulfurs bind in the middle hollow site of the small (100) facets, and on the (111) facets their arrangement is hexagonally distorted with the atoms located in the middle as well as off the hollow sites (but not in the on-top positions). The sulfur arrangement occurs in two alternating inequivalent geometries on adjoining (111) facets. On the other hand on the Au_{201} cluster (TO, with $(m,n) = (3,3)$, see right inset) the sulfur atoms are arranged with the same hexagonal pattern on all the (111) facets (with the central atom adsorbed in the on-top site), and on the (100) facet they form a rhombus with the atoms adsorbed off the hollow sites. From these structures we find that at the mean radius of the sulfur atoms positions, measured from the center of the underlying Au_{140} crystallite (approximately 0.9 Å larger than the mean radius of the faceted crystallite), the packing density is ∼30% larger than on a flat Au(111) surface, corresponding to ∼12% contraction of the mean nearest-neighbor distance between adsorbed sulfur atoms; this is in agreement with the weighted average of the inequivalent sulfur−sulfur distances obtained directly from our determined structures shown in Figure 2 (when referenced to the surface area of the gold crystallite, the sulfur packing density is ∼50% higher than that on a planar Au(111) surface[21]).

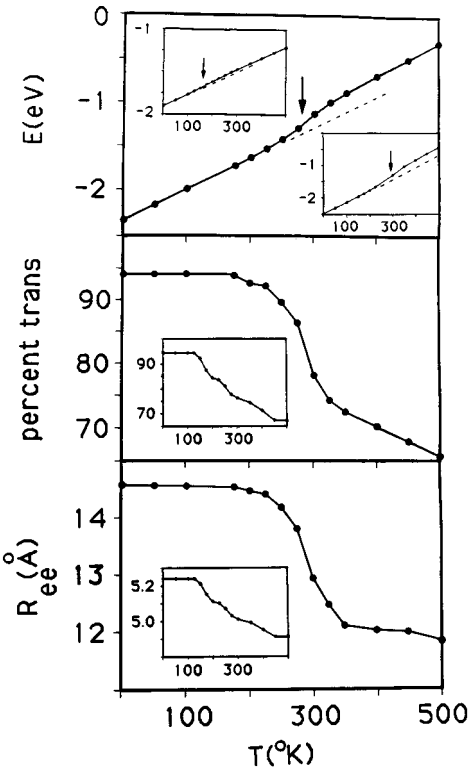

Figure 3. Caloric curves (total energy, E, versus temperature, T), percent trans conformations, and molecular end-to-end length, top to bottom, respectively, for $Au_{140}(RS)_{62}$, obtained via MD simulations. The results in the main figure correspond to dodecanethiols ($R = C_{12}H_{25}$), and those in the upper left insets to butanethiol ($R = C_4H_9$). The caloric curve shown in the right inset to the top frame corresponds to $Au_{586}(C_{12}H_{25}S)_{156}$. The temperatures corresponding to the inflection points in the caloric curves are denoted by arrows. Energy, length, and temperature in units of eV, Å, and degrees kelvin, respectively.

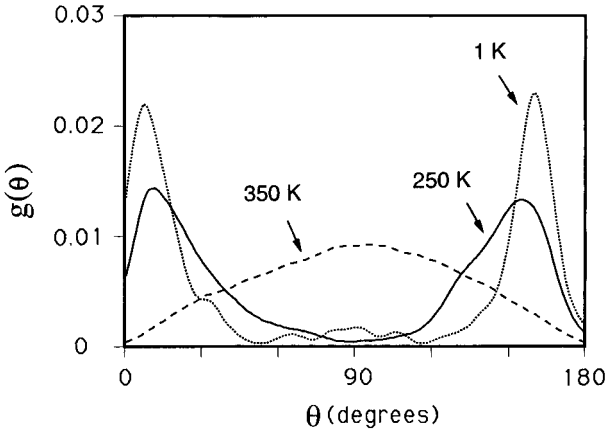

Figure 4. Normalized intermolecular angle distribution, $g(\theta)$ for $Au_{140}(C_{12}H_{25}S)_{62}$ obtained from simulations at $T = 350$, 250, and 1 K showing the development of "anti-parallel" molecular bundles below the melting temperature of the passivating monolayers.

Starting at $T = 500$ K, the passivated clusters were cooled in several stages. Representative caloric curves (total energy versus temperature), along with records of several characteristic properties are shown in Figure 3 for $Au_{140}(RS)_{62}$, $R = C_4H_9$ and $C_{12}H_{25}$. For both thiols, the clear signatures of a first-order phase transition seen in the caloric curves are accompanied by intramolecular conformational changes, portrayed by sharp variations in the percent trans conformations and the end-to-

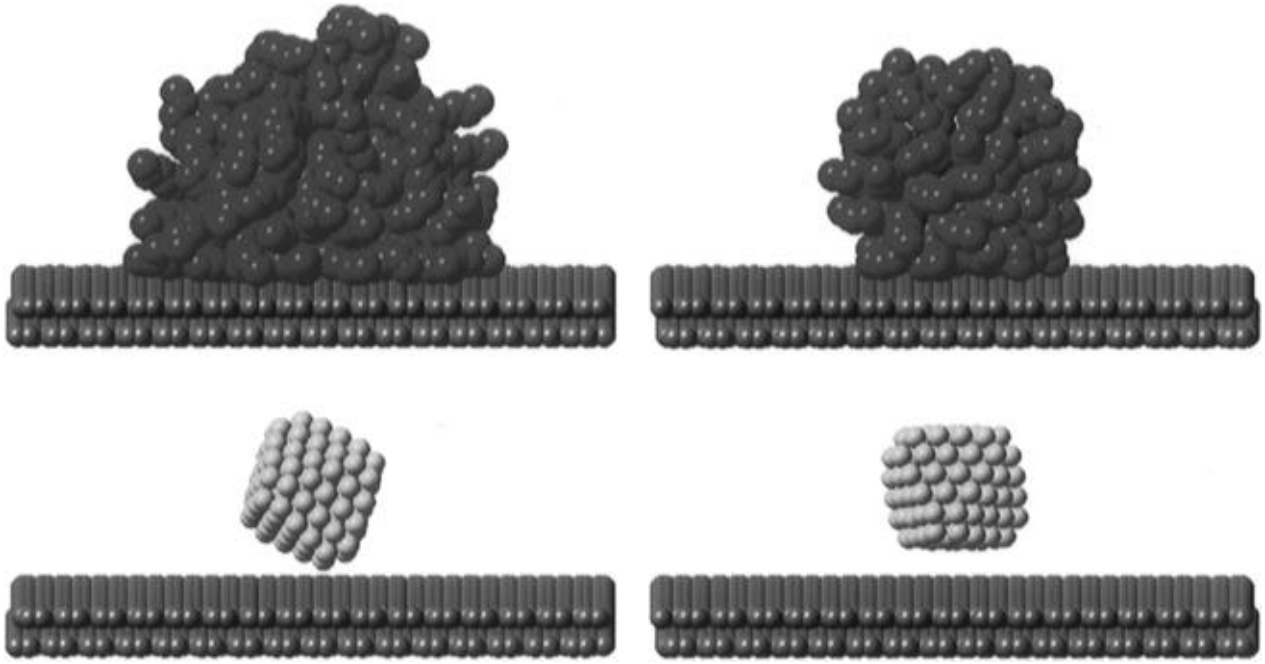

Figure 5. Equilibrium configurations of $Au_{140}(C_{12}H_{25}S)_{62}$ and $Au_{140}(C_4H_9S)_{62}$ adsorbed on graphite, left and right, respectively. In each case a view of the passivated crystallite and that of the underlying Au_{140} crystallite (with the thiols removed) are shown at top and bottom, respectively. Gold and graphite atoms are depicted by yellow and gray spheres, respectively, and alkyl segments by green ones.

end length of the molecules. The melting temperatures, T_M(SAM), are ~160 K (for R = C_4H_9) and 280 K (for R = $C_{12}H_{25}$), and the latent heats of melting (per thiol molecule) are 1.5 and 20 kJ/mol, respectively. Similar results were obtained (see right inset at the top frame of Figure 3) for $Au_N(RS)_M$ with $(N,M) = (201,80)$, (459,136), and (586,156) (the optimal structure of Au_{459} is designated as TO^+ with $(n,m) = (5,3)$ and that of Au_{586} is a TO with $(n,m) = (4,4)$). The melting temperatures we predict for the passivating monolayers of the nanocrystallites are close to (somewhat higher than) those of the corresponding (bulk) alkyl residues ($T_M(C_4H_{10}) = 157$ K and $T_M(C_{12}H_{26}) = 263$ K), while SAMs of alkyl thiols on extended gold surfaces melt at about 60 °C above T_M.[22] Consequently, we conclude that the thermodynamic properties of such monolayers are markedly influenced by the finite size of the underlying surfaces of the nanocrystallite.

The "melting" transition of the passivating monolayers is also reflected in changes in the intermolecular structure. This is particularly significant for longer chain molecular layers. At ow temperatures ($T < T_M$(SAM)) the molecules form "bundles" preferentially oriented with respect to each other; see Figure 1, and the time-averaged normalized distribution, $g(\theta)$, of the intermolecular angle between the end-to-end vectors of the thiol molecules shown in Figure 4. Passivating monolayers made of shorter chains (for example, R = C_4H_9) also exhibit intermolecular order on the (111) and (100) facets at temperatures below the melting transition. There one finds many small ordered domains rather than a few large bundles which develop as the ratio of the chain length to the cluster size increases.

Adsorption Geometries and Surface Mobilities. The equilibrium geometries of $Au_{140}(C_4H_9S)_{62}$ and $Au_{140}(C_{12}H_{25}S)_{62}$ adsorbed on the basal plane of graphite are shown in Figure 5. The short-chain thiols form a more uniform passivating layer allowing the graphite surface to "sense" more directly the flat (111) facets of the Au_{140} nanocrystallite resulting in the (111) facet being oriented parallel to the graphite surface at a distance of 6.9 Å between the gold facet and graphite atoms. On the other hand, the longer chain thiols sweep away from edges and corners of the underlying gold crystallite like "parting hair",

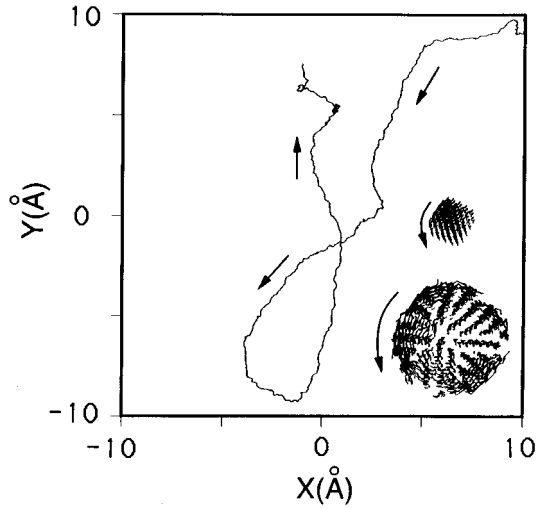

Figure 6. Trajectory of the center of mass of $Au_{140}(C_{12}H_{25}S)_{62}$ recorded in a 1 ns simulation of the nanocrystallite on the basal plane of graphite at $T = 300$ K. Insets illustrate short-time trajectories of the cluster during a typical diffusive event; in the lower inset a view from above of the thiol molecules in the interfacial region is shown and trajectories of only the gold atoms are displayed in the upper inset.

maximizing the interactions between the alkyl groups and the surface, resulting in a smaller separation of the gold crystallite from the graphite surface (5.8 Å), and the gold crystallite is oriented "on edge". In some circumstances, depending on the chain length and on the substrate material, the longer thiols may therefore provide a less protective coating, i.e., reduced screening of the interactions between the gold crystallite and the adsorbing surface, which may lead to stronger adhesion (perhaps even sintering) between the gold crystallite and the substrate. Indeed, increasing the strength of the interaction between the alkyl segments and the surface atoms by a factor of five (corresponding to adsorption on a typical metal surface[17]) resulted in a significant contraction of the distances between the nearest gold-core atoms and surface (3.8 Å for the dodecanethiol case and 6.0 Å for the shorter passivating molecules). The predicted dependence of the adsorption

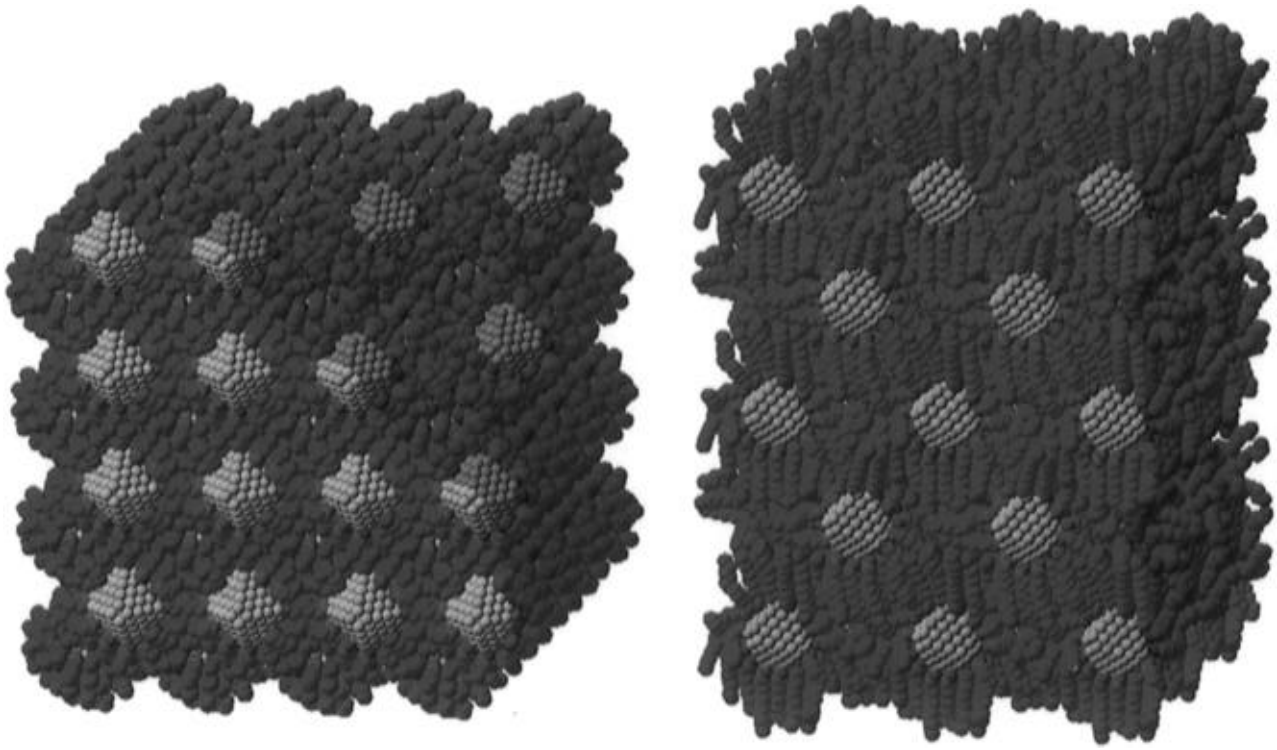

Figure 7. Equilibrium structures of three-dimensional superlattices at 300 K. On the left we show a body-centered cubic superlattice made of $Au_{140}(C_4H_9S)_{62}$ clusters, exposing {100} faces and a corner-cut exposing a (111) face. On the right a tetragonally distorted face-centered cubic, t-fcc, superlattice made of $Au_{140}(C_{12}H_{25}S)_{62}$ clusters is shown, exposing a (100) face. Note the preferential aligned molecular bundles and their "interlocking". Gold atoms are depicted as yellow spheres, alkyl segment in green, and sulfur atoms in red.

geometry of individual nanocrystallites on the length of the passivating molecules, as well as the disruption in the thiol chains packing geometry due to their propensity to adsorb to the surface (see Figures 5 and 6, inset), are likely to affect the structure of ordered adsorbed thin films made of these materials.

The passivating monolayers lubricate the interface between the surface and the crystallites, resulting in high surface mobilities even at low temperatures (see below). The surface diffusion trajectories of the nanocrystallites are characterized by long "flights" interrupted by a change in direction; see Figure 6 for $Au_{140}(C_{12}H_{25}S)_{62}$ at $T = 300$ K. The surface diffusion constant obtained from the data shown in Figure 6 is estimated to be 1.5×10^{-5} cm^2/s, which is similar to the room-temperature diffusion constant of bulk liquid alkanes.[17] Because of the predicted high surface mobilities of the adsorbed passivated clusters, they are likely to be found primarily at pinning sites, such as steps, consistent with recent experimental observations.[5]

The diffusive motion of the massive passivated gold clusters (~40 000 amu) occurs via slip of the interfacial passivating thiols on the graphite surface, which often involves coupled lateral rotation and translation where the thiol chains move in a cooperative manner ("pivoted-slip"; see inset in Figure 6), with the gold nanocrystallite maintaining on average its orientation with respect to the surface (that is, no rolling occurs). To first approximation pertinent features of this cooperative type of "slip-diffusion" may be explained using a simple model. The occurrence of slip requires that the effective lateral shear stress, $\sigma_{||}$, associated with thermal vibrations of the cluster center of mass (ccm, i.e., lateral restoring force divided by the contact area, S, of the thiols with the graphite surface) exceeds a critical value. From our simulations at low temperature, we determined that for $Au_{140}(C_{12}H_{25}S)_{62}$ the effective ccm spring constants for lateral and vertical vibrations are $k_{||} = 0.03$ mdyn/Å and $k_{\perp} = 0.7$ mdyn/Å, respectively (with vibrational periods of $\tau_{||} = 30$ ps and $\tau_{\perp} = 6$ ps, respectively). This leads to an estimate of the maximal lateral vibrational restoring stress $\sigma_{||m} = (2k_{||}k_BT)^{1/2}/S$, where k_B is the Boltzmann constant. The critical lateral shear stress for slip, σ_c, was determined in a separate simulation by applying to the adsorbed cluster a progressively increasing uniform force until slip was initiated, yielding $\sigma_c \simeq 10$ MPa. From $\sigma_{||m} = \sigma_c$ with S = 1200 Å^2, the temperature, T_s, at which significant slip, and thus enhanced diffusive motion, could be initiated may be estimated, yielding $T_s \simeq 200$ K for the longer thiols. For the $Au_{140}(C_4H_9S)_{62}$ adsorbed cluster we determined that $k_{||} = 0.006$ mdyn/Å, $k_{\perp} = 0.5$ mdyn/Å, $\tau_{||} = 60$ ps, $\tau_{\perp} = 7$ ps, $S = 370$ Å^2, and $\sigma_c = 10$ MPa, yielding $T_s = 80$ K. Below the temperature T_s the clusters display slip but much less frequently and T_s, in analogy with conventional descriptions of diffusion, may be interpreted as the temperature for which the thermal energy of the diffusing entity equals or exceeds the energy barrier for motion between neighboring potential wells. These simple estimates for initiating enhanced diffusional motion agree with our observations of the temperatures for which enhanced surface diffusion of the clusters occurred. Moreover, the "frictionless" long flights which the clusters execute on the graphite surface (Figure 6) indicate that once the cooperative diffusional degrees of freedom have been activated, redistribution of the energy into other degrees of freedom of the diffusing cluster is slow. Consequently, the diffusive motion persists with only a small degree of dissipation from the diffusion-active modes. At elevated temperatures the high surface mobility of the passivated clusters may reduce due to thermal agitation of the passivating molecules and loss of cooperativity of the displacement process. The mechanism and rate of diffusion are likely to depend on the strength of interaction between the chain segments and the adsorbing surface relative to the magnitude of the intermolecular interactions. These interactions affect the diffusion barrier height, as well as the degree of cooperativity between the interfacial passivating molecules.

Structures and Transformations of 3D Superlattices. Using constant-pressure simulations with the vectors defining

the periodic calculational cell (consisting of four $Au_{140}(C_4H_9S)_{62}$ crystallites) treated dynamically,[23] we predict that at room temperature a superlattice bcc crystal with a lattice constant a(bcc) = 29.2 Å is formed, and the individual crystallites are oriented with the axes along the bcc superlattice directions (see Figure 7). This structure is predicted to transform reversibly to a fcc (or a hcp) lattice upon heating to 350 K, with a lattice constant of a(fcc) = 38 Å, and the individual crystallites display a significantly increased orientational freedom, possibly associated with orientational melting. (When bringing the fcc superlattice back to T = 300 K, the transformation to a bcc structure occurred after 3−6 ns, which is a rather long time on the scale of MD simulations.) In the equilibrium configuration of the superlattices, the short-chain passivating molecules are much above their melting temperature and are not ordered or bundled along specific directions but are in a liquidlike state. At T = 300 K the total energy of the bcc structure is lower by 0.26% (0.25 eV = 24 kJ/mol, per passivated crystallite) than that of the fcc one. In these simulations the interactions between the passivated nanocrystallites were augmented by van der Waals (vdW) interactions[24] between the gold cores. The dominant contribution to the intercrystallite potential energy comes from direct interaction between the passivating molecules and the relative contribution of the gold core−core vdW interaction to the intercrystallite potential energy (per nanocrystallite) is ∼1%. The cohesive energies (the difference between the total energy of the isolated cluster and its energy in the superlattice) of the bcc and fcc superlattices were determined to be 4.1 eV (at 300 K) and 3.2 eV (at 350 K), respectively. These large cohesive energies (as well as that for the superlattice made of gold clusters passivated by longer-chain molecules, see below) imply that at high temperatures one may form molecular liquids of these materials.

While as aforementioned at room temperature Au_{140} nanocrystallites passivated by short-chain thiols form a bcc superlattice transforming to a fcc structure upon heating, nanocrystallites of a more spherical morphology may form fcc superlattices even at room temperature. Furthermore, passivation of nanocrystallites by long-chain molecules can result in the formation of superlattice structures different from those occurring for short-chain ones under the same conditions; such structures may include tetragonally distorted superlattices, particularly at lower temperatures, when the passivating molecules show a large tendency to form oriented bundled structures. Indeed, our simulations of the 3D superlattice made of $Au_{140}(C_{12}H_{25}S)_{62}$ show formation of a tetragonally distorted fcc structure at T = 300 K (lattice constants $a = b$ = 43 Å and c = 51 Å). In this structure the superlattice environment induces an enhanced degree of preferential arrangement of the dodecane thiols into "antiparallel" bundles oriented along the c(001) direction which interlock (without interdigitation of individual molecules) to form the ordered superlattice (see Figure 7). The dimensions of the c and a axes of the superlattice correspond approximately to the length and twice the width of the bundled passivated cluster, respectively. The cohesive energy of the superlattice is 15.0 eV/cluster and is dominated by the vdW interaction between the bundles of the passivating molecules. These results also suggest that when forming adsorbed thin films the molecular bundles will tend to orient parallel to the substrate due to the attraction between the passivating molecules and the surface atoms. We expect that in such an arrangement the c axis of the adsorbed ordered thin film will lie in the plane of the adsorbing surface exposing a (100) face of the t-fcc structure (since $c > a$, an image of the thin-film structure taken from above may appear to be that of a bcc lattice viewed along the (110) direction).

Typical vibrational periods of the massive gold cores in these superlattice systems are ∼10−20 ps (that is, frequencies in the range ∼1−3 cm^{-1}), similar to those of the clusters adsorbed on the graphite surface. Note that in the case of the adsorbed clusters, when the temperature exceeds the critical temperature for slip, T_s, one expects, and indeed we find, that the increased degree of interfacial slip is accompanied by a marked attenuation of the lateral vibrational modes of the adsorbed cluster due to a decrease of the restorting force.

The general character of the intermolecular organization of the surfactant chains and the nature of the structures and bonding in the superlattice assemblies suggest correspondences with investigations of other systems involving similar structures, such as inverse micelles,[25] liquid crystals,[26] and lipids.[27] For example, it is interesting to note that viewed in one of the closed-packed planes of the t-fcc lattice, the bundled passivated clusters resemble certain hexatic liquid-crystal phases (hexatic phases[26]) where hexagonally arranged rodlike molecules tilt in the direction of the next-nearest neighbors (that is, in the direction of the midpoint of the bond connecting adjacent neighbors). Also, the interlocking of the passivated nanocrystallites in the t-fcc lattice is a higher dimensional analogue of the 2D ribbon phases of certain sodium soaps.[27]

Our results pertaining to the structure, dynamics, and thermodynamics of passivated gold nanocrystallites provide significant insights into the nature of these systems in different environments. In particular we showed that the finite size of the core metal crystallites confers to the passivating molecular layers unique structural properties (oriented molecular bundles) which govern (through bundle interlocking) the organization of the particles into crystalline superlattices. Additionally, these molecular structures were found to exhibit thermodynamic melting transitions accompanied by intramolecular conformational transformations. Furthermore, we have shown that on a graphite surface these heavy particles (with masses exceeding 40 000 amu) diffuse at a surprisingly high rate ($D \approx 10^{-5}$ cm^2/s), with the passivating molecules lubricating the interface and participating in an activated collective slip-diffusion mechanism characterized by small frictional dissipation. These results demonstrate that the properties of such systems (as well as other materials such as semiconductors[8]) can be modified (controlled) through selection of the sizes of the nanocrystallites and/or length of the passivating molecules (the effective control parameter is the ratio between the length of the passivating molecules and the dimension of the core nanocrystallite) and that they may be varied through changes in the mode and degree of aggregation (that is, isolated clusters in the gas phase or in solution, clusters adsorbed on surfaces, 2D films, and 3D superlattices), as well as through variations in the temperature. Coupled with further development of preparation and characterization methods, this study motivates and suggests new avenues and phenomena for investigation and potential utilization of these novel materials.

Acknowledgment. This research is supported by the U.S. Department of Energy and the AFOSR. Calculations were performed on Cray Computers at the National Energy Research Supercomputer Center, Livermore, California, and at the Georgia Institute of Technology Center for Computational Materials Science. Dr. Charles Cleveland is gratefully acknowledged for his assistance in preparation of the color figures. Collaborative research with R. L. Whetten and his experimental group on nanocrystal systems is acknowledged (see refs 4 and 9).

References and Notes

(1) See articles in: *Clusters of Atoms and Molecules*, Haberland, H., Ed.; Springer Series in Chem. Phys. 52 and 57; Springer: Berlin, 1994.

(2) Brust, M.; Walker, M.; Bethell, D.; Schriffin, D. J.; Whyman, R. *J. Chem. Soc., Chem. Commun.* **1994**, 801.

(3) Brust, M.; Bethell, D.; Schriffin, D. J.; Kiely, C. J. *Adv. Mater.* **1995**, *7*, 795.

(4) Whetten, R. L.; Khoury, J. T.; Alvarez, M.; Murthy, S.; Vezmar, I.; Wang, Z. L.; Stephens, P. W.; Cleveland, C. L.; Luedtke, W. D.; Landman, U. *Adv. Mater.* **1996**, *8*, 428. See also Whetten, R. L.; et al. In *Chemical Physics of Fullerenes 5 and 10 Years Later*; Andreoni, W., Ed.; Kluwer: Dordrecht, 1996; p 475.

(5) Terrill, R. H.; et al. *J. Am. Chem. Soc.* **1995**, *117*, 12537.

(6) O'hara, P. C.; Leff, D. V.; Heath, J. R.; Gelbart, W. M. *Phys. Rev. Lett.* **1995**, *75*, 3466.

(7) Dorogi, M.; Gomez, J.; Osifchin, R.; Andres, R. P.; Reifenberger, R. *Phys. Rev.* **1995**, *B52*, 9071.

(8) While our focus here in on metal (gold) nanocrystals significant advances have been made in this area for semiconductor materials. For a recent review see: Alivisatos, A. P. *Science* **1996**, *271*, 933. See also: Murray, C. B.; Kagan, C. R.; Bawendi, M. G. *Science* **1995**, *270*, 1335.

(9) Cleveland, C. L.; Landman, U., to be published; the optimal structures of the gold cores were taken as those determined through simulations of bare gold clusters. Mass spectrometry, transmission electron microscopy, and X-ray measurements performed on isolated fractions of solution-phase prepared passivated gold crystallites,[4] confirmed that the structures of the gold cores of dodecane thiol passivated clusters are the same as those predicted in the simulations. See also Cleveland, C. L.; Landman, U.; Shafigullin, M.; Stephens, P. W.; Whetten, R. L. *Z. Phys. D.*, in press.

(10) See: Ulman, A. *An Introduction to Ultrathin Organic Films*; Academic Press: San Diego, CA, 1991.

(11) Dubois, L. H.; Nuzzo, R. G. *Annu. Rev. Phys. Chem.* **1992**, *43*, 437. Nuzzo, R. G.; Allara, D. L. *J. Am. Chem. Soc.* **1983**, *105*, 4481.

(12) See list of references in ref 1 of: Terrill, R. H.; et al., ref 5. See also: Fenter, P.; Eberhardt, A.; Eisenberger, P. *Science* **1994**, *266*, 1216 and references therein.

(13) Hautman, J.; Klein, M. L. *J. Chem. Phys.* **1989**, *91*, 4994.

(14) Jorgensen, W. L.; Madura, J. D.; Swenson, C. J. *J. Am. Chem. Soc.* **1984**, *106*, 6638, supplemented by angle bending potentials following: Ploeg, P.; Berendsen, H. J. C. *J. Chem. Phys.* **1982**, *76*, 3271.

(15) Sellers, H.; Ulman, A.; Shnidman, Y.; Eilers, J. E. *J. Am. Chem. Soc.* **1993**, *115*, 9389.

(16) Jorgensen, W. L. *J. Phys. Chem.* **1986**, *90*, 6379, with modifications similar to those in ref 13.

(17) Xia, T. K.; Ouyang, J.; Ribarsky, M. W.; Landman, U. *Phys. Rev. Lett.* **1992**, *69*, 1967.

(18) The parametrization used is after: Adams, J. B.; Foiles, S. M.; Wolfer, W. G. *J. Mater. Res.* **1989**, *4*, 102. See also: Cleveland, C. L.; Landman, U. *J. Chem. Phys.* **1991**, *94*, 7376.

(19) Leggetter, S.; Tildesley, D. J. *Mol. Phys.* **1989**, *68*, 519.

(20) Strong, L.; Whitesides, G. M. *Langmuir* **1988**, *4*, 546.

(21) A similar result has been reached on the basis of geometric arguments and elemental analysis in ref 2; see also an estimate based on a simple model in: Leff, D. V.; Ohara, P. C.; Heath, J.; Gelbart, W. M. *J. Phys. Chem.* **1995**, *99*, 7036.

(22) Fenter, P.; Eisenberger, P.; Liang, K. L. *Phys. Rev. Lett.* **1993**, *70*, 2447.

(23) Parrinello, M.; Rahman, A. *Phys. Rev. Lett.* **1980**, *45*, 1196.

(24) In these calculations we used the expression given in: Hamaker, H. C. *Physica* **1937**, *4*, 1058. The Hamaker constant for gold−gold attraction through dodecane is ≈2 eV (see also ref 6), using data given in Bargeman, D.; Van Voorst Vaden, F. *J. Electroanal. Chem.* **1972**, *37*, 45. Israelachvili, J. N. *Intermolecular and Surface Forces*; Academic Press: New York, 1992.

(25) Gompper, G.; Schick, M. *Self Assembly of Amphiphilic Systems.* In *Phase Transitions and Critical Phenomena*; Academic: London, 1994; Vol. 16.

(26) Chaikin, P. M.; Lubensky, T. C. *Principles of Condensed Matter Physics*; Cambridge University Press: Cambridge, 1995. de Gennes, P.-G.; Prost, J. *The Physics of Liquid Crystals*; Clarendon Press: Oxford, 1993.

(27) Small, D. M. *The Physical Chemistry of Lipids*; Plenum: New York, 1986.

JP961721G